

Article

# Simple and Rapid Synthesis of Organically Modified Natural Acid Clay for the Adsorption of Anionic and Cationic Dyes

Tomohiro Iwasaki 

Department of Chemical Engineering, Osaka Metropolitan University, Osaka 599-8531, Japan; tomohiro.iwasaki@omu.ac.jp

**Abstract:** A simple method for organically modifying a natural acid clay (Japanese acid clay) rapidly with alkylamine has been developed. Japanese acid clay mainly consists of acidic montmorillonite and was successfully modified with decylamine in water at room temperature for a short time period (10 min) using an ultrasonic bath without any pretreatments. The structure of the modified clay changed from exterior surface modification to intercalation with an increase in the decylamine content. The equilibrium adsorption capacity for the anionic dye methyl orange (MO) increased with increasing decylamine content. The adsorption kinetics and isotherm were well described by the pseudo-second-order and Langmuir models, respectively. Better MO adsorption was obtained under the conditions of high dosage, low pH value, and low temperature. The adsorbent was also found to have good adsorption for not only MO but also other anionic dyes (Congo red and eosin Y) and cationic dyes (methylene blue, crystal violet, and rhodamine B). In particular, the decylamine-intercalated clay adsorbent exhibited a high level of adsorption capacity for Congo red and crystal violet. The results demonstrate that the synthesis process can provide a simple and cost-effective organoclay as an adsorbent with high performance for the removal of anionic and cationic dyes.

**Keywords:** Japanese acid clay; decylamine; organoclay; surface modification; intercalation; dye adsorption removal



**Citation:** Iwasaki, T. Simple and Rapid Synthesis of Organically Modified Natural Acid Clay for the Adsorption of Anionic and Cationic Dyes. *Minerals* **2023**, *13*, 41. <https://doi.org/10.3390/min13010041>

Academic Editors: Michal Slaný and Itamar Shabtai

Received: 19 November 2022

Revised: 24 December 2022

Accepted: 24 December 2022

Published: 27 December 2022



**Copyright:** © 2022 by the author. Licensee MDPI, Basel, Switzerland. This article is an open access article distributed under the terms and conditions of the Creative Commons Attribution (CC BY) license (<https://creativecommons.org/licenses/by/4.0/>).

## 1. Introduction

Removal of toxic organic pollutants from wastewater is critical to achieving the United Nations Sustainable Development Goals (UN SDGs) aimed at the realization of a sustainable society [1–3]. Among treatments of industrially discharged organic pollutants, the purification of wastewater containing synthetic dyes from dye production and dyeing processes is still a challenging issue [4]. To remove dyes efficiently from aqueous solutions, adsorption is widely and frequently employed due to easy operation and low energy consumption [5,6], and various adsorbents, such as activated carbon, zeolite, and metal-organic frameworks (MOFs), have been developed [7–12]. However, to enhance adsorption performance through pore development and surface activation, energy consumption and process costs can often increase [13]. Therefore, the development of a synthesis process for obtaining cost-effective adsorbents with high adsorption performance at low environmental impacts in production is needed.

Recently, organoclays, in which clays or layered (alumino-) silicates are modified with organic compounds, have attracted much attention for use as adsorbents for dye removal [14–25] because they can be relatively easily prepared under environmentally friendly conditions. In this study, an organoclay adsorbent using an inexpensive natural acid clay, Japanese acid clay [26–28] (which is a name for fuller's earth yielded in Japan), has been newly developed. This acidic clay mainly consists of calcium-type montmorillonite and the montmorillonite layers have protons instead of sodium ions; namely, this clay is similar to acidic bentonite clay in which sodium ions are ion-exchanged with protons. The acidic clay is non-swelling in water, unlike normal bentonite clay. Decylamine was

employed as the organic modifier of the acid clay [29], and the cost-effective organoclay adsorbent can be quite easily synthesized without heating (i.e., at room temperature) for a short time period. This results in the exterior surface modification and intercalation of the acid clay with decylamine [29]. The structural change of organoclay with this modification was investigated, and the dye adsorption properties were studied.

## 2. Materials and Methods

### 2.1. Synthesis and Characterization of Organoclays

Japanese acid clay and decylamine (DA) were purchased from Kishida Chemical (Sanda, Japan) and FUJIFILM Wako Pure Chemical (Osaka, Japan), respectively, and used without further purification. The cation exchange capacity (CEC) is approximately 10 cmol/kg. The chemical composition determined by energy dispersive X-ray spectroscopy (EDX; Epsilon 1, Malvern Panalytical, Malvern, UK) is as follows: 55.5 wt% SiO<sub>2</sub>, 11.2 wt% Al<sub>2</sub>O<sub>3</sub>, 2.7 wt% Fe<sub>2</sub>O<sub>3</sub>, and 0.9 wt% CaO, which is similar to normal bentonite.

Briefly, 0.1 g of Japanese acid clay powder was added to 20 g of deionized water in a glass tube with a screw cap. The aggregates of clay particles were disintegrated in an ultrasonic bath (40 kHz, 200 W) for 10 min. A predetermined amount of DA was added to the suspension and the DA-containing suspension was vigorously shaken at room temperature in the ultrasonic bath for 10 min. The clay particles modified with DA were filtered and dried at room temperature overnight. The organoclay samples were used for further characterization and dye adsorption study. In this work, five organoclay samples with different DA contents (4.5, 9.3, 16.2, 20.0, and 25.6 mass%, denoted as DA1, DA2, DA3, DA4, and DA5, respectively) were prepared. The DA contents were determined by thermogravimetry/differential thermogravimetric analysis (TG/DTA; DTG-60, Shimadzu, Kyoto, Japan) at a heating rate of 10 K/min under airflow (100 mL/min), assuming that the adsorbed water was eliminated below 120 °C based on the TG data of the original clay. The pristine (unmodified) clay was represented as DA0.

The structures of the samples were confirmed by a powder X-ray diffractometer (XRD-6100, Shimadzu, Kyoto, Japan; CuK $\alpha$ , wavelength = 0.154 nm, 30 mA, 30 kV, 1°/min). The morphologies of representative samples were observed with a field-emission scanning electron microscope (FE-SEM; JSM-6700F, JEOL, Tokyo, Japan) at 15 kV. The nitrogen adsorption-desorption isotherms were also measured at 77 K using nitrogen adsorption analysis (BELSORP MAX G, MicrotracBEL, Osaka, Japan) to determine the specific surface area and pore size distribution calculated using the Brunauer–Emmett–Teller (BET) and Barrett–Joyner–Halenda (BJH) methods, respectively.

### 2.2. Dye Adsorption Study

The anionic and cationic dyes used in this work are listed in Table 1. To study the effects of the organoclay structure on the dye adsorption properties, anionic methyl orange (MO) dye, which is widely used as a model adsorbate to evaluate the adsorption properties of various adsorbents, was selected. The adsorption experiments were performed in batch mode. Typically, 10 mg of an organoclay sample as the adsorbent was added to 20 mL of the MO solution with a concentration of 20 mg/L. The adsorbents were used without selecting a specified grain fraction of the sample powders. The suspension was vigorously stirred at room temperature for a proper amount of time. After that, the adsorbent was centrifuged and the supernatant was collected to measure the concentration. The absorbance was measured with a spectrophotometer (U-2900, Hitachi High-Technologies, Tokyo, Japan) at the wavelength shown in Table 1. The MO concentration was determined using a calibration curve prepared in advance. The adsorbed amount of MO at a specified time was calculated by Equation (1).

$$q_t = \frac{(C_0 - C_t)V}{m} \quad (1)$$

where  $q_t$  (mg/g) is the adsorbed MO amount at a contact time  $t$  (h),  $C_0$  and  $C_t$  (mg/L) are the MO concentrations of the solutions before and after contact, respectively,  $V$  (L) is the

volume of the solution, and  $m$  (g) is the mass of the adsorbent. To study the adsorption kinetics, the contact time was varied from 15 min to 4 h. The equilibrium adsorption capacity  $q_e$  (mg/g) was calculated from the equilibrium concentration  $C_e$  (mg/L) obtained after contact for more than 24 h using Equation (1). In addition, the adsorbent dosage ( $= m/V$ ), initial solution pH, and temperature were also varied between 0.24 g/L and 1.5 g/L, between 3.1 and 10.9, and between 301 K and 333 K, respectively. The pH was adjusted by using 0.1 mol/L HCl and 0.1 mol/L NaOH solutions. Furthermore, to investigate the adsorption properties of various dyes, experiments using several anionic (Congo red and eosin Y) and cationic (methylene blue, crystal violet, and rhodamine B) dyes were also conducted. In the adsorption experiments, the initial dye concentrations were varied as shown in Table 1, and the adsorption isotherms were analyzed. The reproducibility of each adsorption as well as the synthesis of organoclay samples was confirmed through repeated experiments. The Fourier transform infrared (FT-IR) spectra of the organoclay powder before and after the adsorption were recorded on a spectrophotometer (IRAffinity-1, Shimadzu, Kyoto, Japan) with the KBr pellet technique. The TG/DTA curves were also measured with the thermal analyzer mentioned above.

**Table 1.** Anionic and cationic dyes used in this work.

Dye	Supplier *	Initial Concentration $C_0$ (mg/L)	Natural pH of 20 mg/L Solution	Wavelength (nm)
Anionic:				
Methyl orange (MO)	KC	20–300	6.9	464
Congo red (CR)	NT	20–600	7.1	498
Eosin Y (EY)	FW	20–100	5.1	517
Cationic:				
Methylene blue (MB)	KC	20–350	5.7	665
Crystal violet (CV)	KC	20–500	5.6	595
Rhodamine B (RB)	FW	20–100	4.8	554

\* KC = Kishida Chemical (Japan), NT = Nacalai Tesque (Japan), FW = FUJIFILM Wako Pure Chemical (Japan).

### 3. Results and Discussion

#### 3.1. Change in the Structure of Organoclay with DA Content

The X-ray diffraction (XRD) pattern and basal spacing of the organoclay samples are shown in Figures 1 and 2, respectively, together with those of the original clay. The original Japanese acid clay (DA0) had a diffraction peak at  $2\theta \approx 6^\circ$ , which almost coincided with acidic (protonated) montmorillonite [30] with a basal spacing of 1.5 nm. When the DA content was 4.5 mass% (i.e., DA1 sample), the crystal structure was almost the same as that of the original, which suggested that the DA molecules adhered onto the exterior surface of clay particles without intercalation into the montmorillonite interlayer spaces. As the DA content was increased, the basal spacing increased due to the intercalation of DA molecules. The DA2 sample (9.3 mass%) had a basal spacing of 1.8 nm, which was similar to the diameter (approximately 0.3 nm) of the DA molecule, which was estimated assuming that the shape of the DA molecule was cylindrical. This suggests that the DA2 sample has a lateral monolayer-type structure [31,32]. The DA3 sample (16.2 mass%) had a broad peak, indicating a disordered structure due to the transition region. In contrast, the diffraction peaks of the DA4 and DA5 samples (20.0 and 25.6 mass%, respectively) were sharp. In particular, the DA5 sample had a well-ordered intercalation structure with a basal spacing of 3.1 nm, suggesting a paraffin-type bilayer structure [31,32].

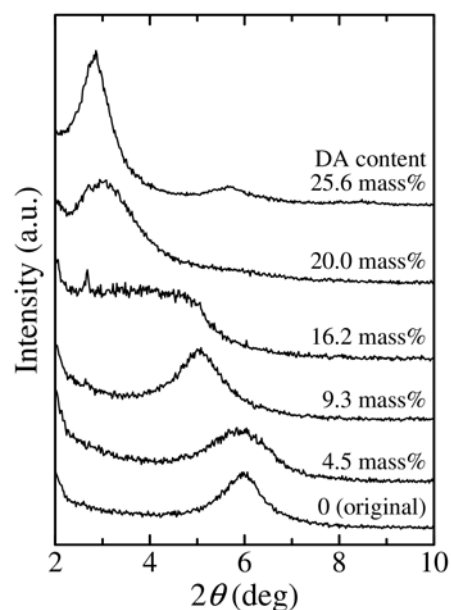


**Figure 1.** XRD patterns of samples with different DA contents.

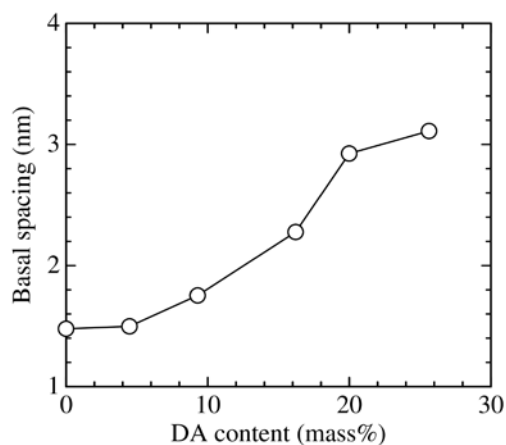


**Figure 2.** Change in basal spacing of samples with DA content.

Typical FE-SEM images of DA0 (pristine), DA1 (exterior surface-modified), and DA5 (intercalated) samples are shown in Figure 3 as representatives. The morphologies of the DA1 sample were almost the same as those of the DA0 sample, which was similar to typical bentonite clays. The particles of the DA5 sample tended to aggregate more strongly. The nitrogen adsorption–desorption isotherms were measured to investigate the changes in the pore structure with surface modification and intercalation. As illustrated in Figure 4, the adsorption–desorption isotherms showed type IV adsorption behavior with a typical H3 hysteresis loop, which can be attributed to the slit-shaped pores of aggregates of plate-shaped particles. The pore size distribution curves are shown in Figure 5. The BET surface area, pore volume, and average pore diameter of the samples are summarized in Table 2. Although the original clay had a relatively large amount of mesopores and a relatively high specific surface area, modification with DA decreased the pore structure. In particular, the micropores and mesopores were drastically decreased by the modification, which may have resulted in a decrease in the specific surface area and pore volume. This result suggests that the DA molecules partially block the micropores and mesopores of the original clay.

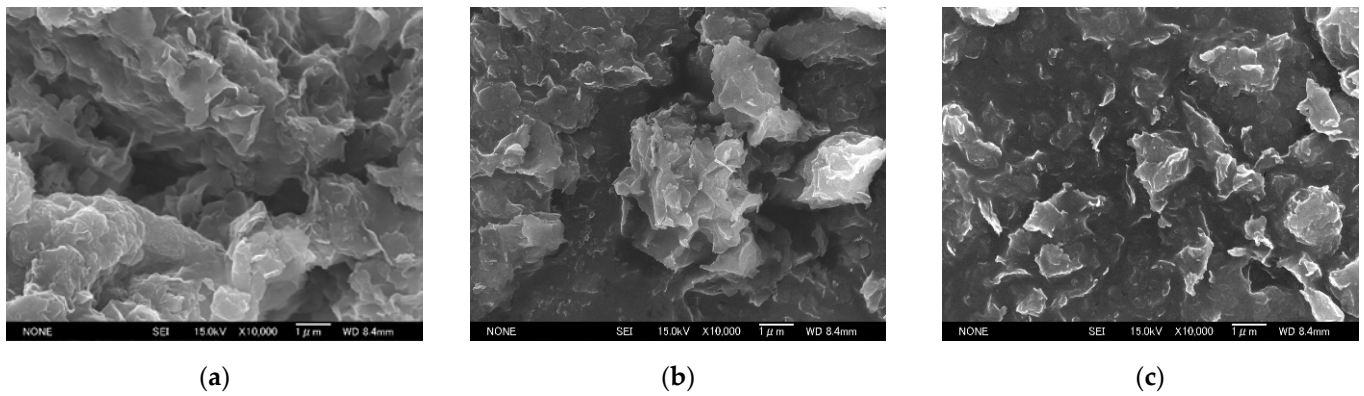


**Figure 3.** Typical SEM images of (a) DA0 (original acid clay), (b) DA1 (surface-modified), and (c) DA5 (intercalated) samples.

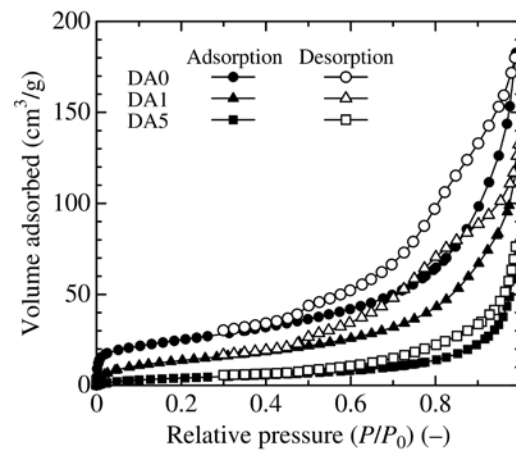


**Figure 4.** Nitrogen adsorption–desorption isotherms of the DA0, DA1, and DA5 samples.

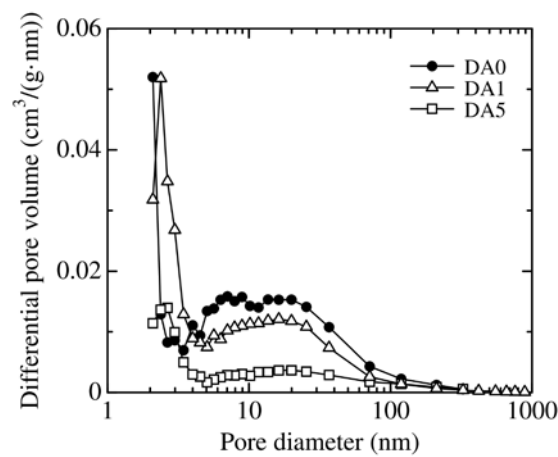


**Figure 5.** Pore diameter distributions of the DA0, DA1, and DA5 samples.

**Table 2.** Specific surface area, pore volume, and pore diameter of the DA0, DA1, and DA5 samples.

Sample	BET Surface Area (m <sup>2</sup> /g)	Pore Volume (cm <sup>3</sup> /g)	Average Pore Diameter (nm)
DA0	87.9	0.278	21.1
DA1	52.1	0.218	18.3
DA5	16.4	0.118	27.8

### 3.2. Effect of Adsorbent Structure on MO Equilibrium Adsorption Capacity

The change in the MO equilibrium adsorption capacity with the DA content of the organoclay samples is illustrated in Figure 6. The equilibrium adsorption capacity drastically increased with increasing DA content below 9.3 mass%, which indicates that the DA molecules in the organoclays act as the adsorption sites for MO. The adsorption capacity reached 36 mg/g at a DA content above 20 mass% (i.e., the DA4 and DA5 samples). However, at higher than 9.3 mass% the increase in the adsorption capacity was slight, which suggested that the rate of effective adsorption sites decreased at high DA contents.

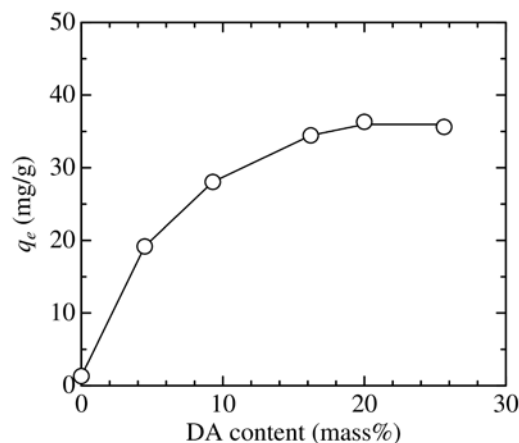


**Figure 6.** Change in MO equilibrium adsorption capacity of samples with DA content (dosage = 0.5 g/L, initial concentration = 20 mg/L, initial pH = 6.9, temperature = 301 K).

The relationship between the equilibrium adsorption capacity and the basal spacing of the samples is shown in Figure 7. Although the DA1 sample (4.5 mass% DA) had almost the same basal spacing as DA0 (original clay), the DA1 sample had a much larger adsorption capacity than DA0 due to surface modification with DA. The DA-intercalated samples with large values of basal spacing possessed relatively large amounts of DA molecules in the interlayer spaces, which resulted in high adsorption capacities. To investigate the effectiveness of DA in MO adsorption, the equilibrium adsorption capacity  $q_e'$  [mg/g-DA] per unit mass of DA was calculated for each organoclay sample. As shown in Figure 8,  $q_e'$  monotonically decreased with increasing DA content, which suggests that DA molecules on the exterior surface of clay particles acted as relatively more effective adsorption sites than in the interlayer spaces.

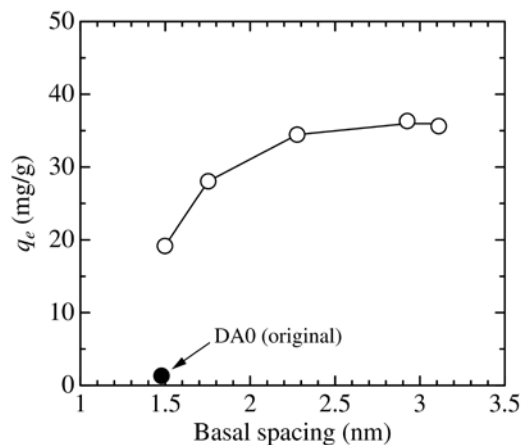


**Figure 7.** Relationship between equilibrium adsorption capacity and basal spacing (dosage = 0.5 g/L, initial concentration = 20 mg/L, initial pH = 6.9, temperature = 301 K).

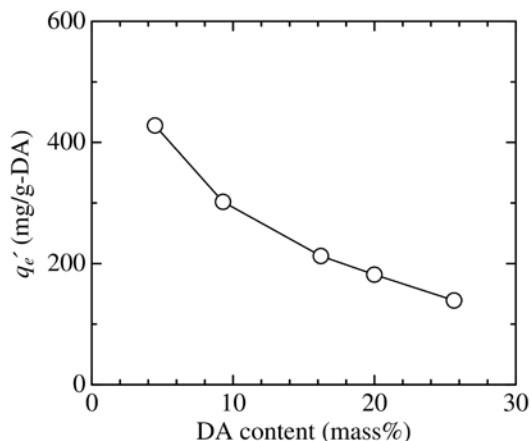


**Figure 8.** MO equilibrium adsorption capacity per unit mass of DA (dosage = 0.5 g/L, initial concentration = 20 mg/L, initial pH = 6.9, temperature = 301 K).

3.3. Dependence of Adsorbent Dosage, pH, and Temperature on MO Removal

The effects of adsorbent dosage, initial pH value, and temperature on the MO equilibrium adsorption capacity and removal efficiency of the DA5 sample, which had the maximal adsorption capacity among the samples, are displayed in Figure 9. With increasing adsorbent dosage, the removal efficiency gradually increased and reached 98% at 1.5 g/L due to an increase in the total surface area of the adsorbent (Figure 9a). However, the equilibrium adsorption capacity decreased as the adsorbent dosage was increased, which suggested a decrease in the rate of effective adsorption sites in the adsorbent.

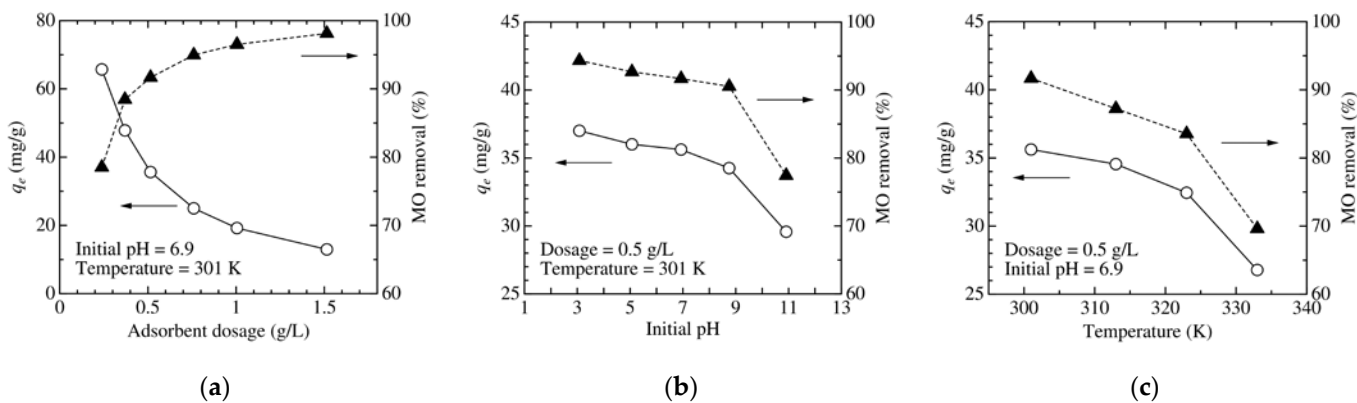


**Figure 9.** Change in MO equilibrium adsorption capacity of the DA5 sample with (a) adsorbent dosage, (b) initial pH, and (c) temperature (initial concentration = 20 mg/L).

Subsequently, as shown in Figure 9b, the equilibrium adsorption capacity and removal efficiency gently decreased with increasing pH, and a relatively low adsorption capacity was observed under basic conditions. MO adsorption with a removal efficiency higher than 90% was achieved under both acidic and neutral conditions.

At low temperatures, the equilibrium adsorption capacity and removal efficiency were relatively high and decreased with increasing temperature (Figure 9c), which suggests that MO adsorption is an exothermic process. Based on the adsorption data obtained at different temperatures, the MO adsorption onto the DA5 sample was thermodynamically analyzed. The Gibbs free energy  $\Delta G^\circ$  (J/mol) is expressed as

$$\Delta G^\circ = \Delta H - T\Delta S^\circ \tag{2}$$

where  $\Delta H^\circ$  (J/mol) is the standard enthalpy,  $\Delta S^\circ$  (J/(mol·K)) is the standard entropy and  $T$  (K) is the absolute temperature. The thermodynamic parameters  $\Delta H^\circ$  and  $\Delta S^\circ$  for adsorption are expressed by the Van 't Hoff equation.

$$\ln K_d = \frac{\Delta S^\circ}{R} - \frac{\Delta H^\circ}{RT} \quad (3)$$

where  $R$  (J/(mol·K)) is the gas constant and  $K_d$  (-) is the distribution coefficient defined by Equation (4) [33].

$$K_d = \frac{q_e m}{C_e V} \quad (4)$$

where  $q_e$  (mg/g) is the equilibrium uptake of MO,  $m$  (g) is the mass of the adsorbent,  $C_e$  (mg/L) is the MO concentration at equilibrium, and  $V$  (L) is the volume of the solution. Using the experimental data shown in Figure 9c,  $\ln K_d$  was plotted against  $1/T$ . As shown in Figure 10, a linear relationship between  $\ln K_d$  and  $1/T$  was obtained. The values of  $\Delta H^\circ$  and  $\Delta S^\circ$  were determined from the slope and intercept, respectively, using Equation (3) and the value of  $\Delta G^\circ$  at each temperature was calculated using Equation (2). The thermodynamic parameters are summarized in Table 3. The values of  $\Delta G^\circ$ ,  $\Delta H^\circ$ , and  $\Delta S^\circ$  were all negative within the temperature range, which suggests the feasibility and spontaneity of the adsorption process, the exothermic adsorption process, and the decrease in randomness at the adsorbent/dye interface during the adsorption process. In addition, large negative values of  $\Delta G^\circ$  at low temperatures suggest that the DA5 sample has a high affinity for MO removal at lower temperatures.

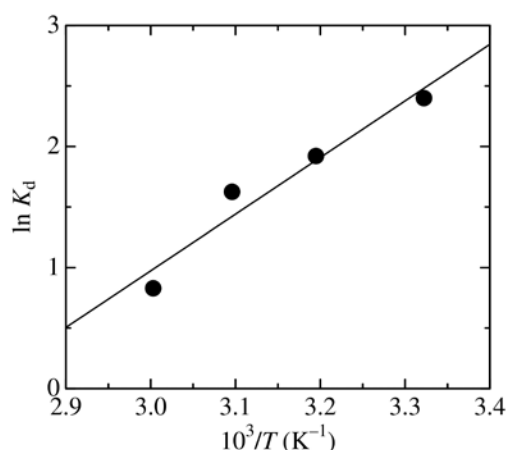


**Figure 10.** Plot of  $\ln K_d$  against  $1/T$  for estimation of thermodynamic parameters for adsorption of MO onto the DA5 sample (dosage = 0.5 g/L, initial concentration = 20 mg/L, initial pH = 6.9).

**Table 3.** Thermodynamic parameters for MO adsorption on the DA5 sample.

Temperature (K)	$\Delta G^\circ$ (kJ/mol)	$\Delta H^\circ$ (kJ/mol)	$\Delta S^\circ$ (kJ/(mol·K))
301	−6.00		
313	−5.00		
323	−4.36	−38.9	−0.109
333	−2.29		

### 3.4. Analysis of Adsorption Kinetics and Isotherm

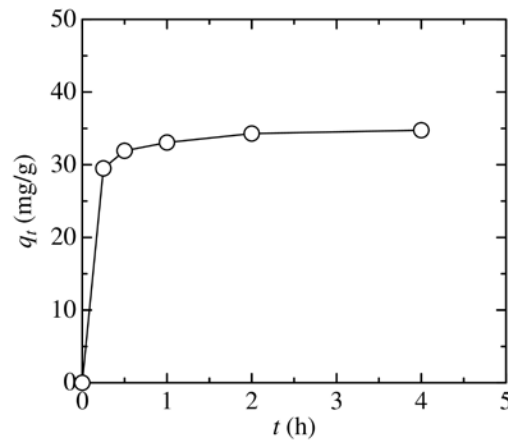
The change in the adsorbed amount of MO with the contact time is illustrated in Figure 11. The adsorbed amount of MO rapidly increased in the initial stage and approximately reached equilibrium after several hours. To investigate the mechanism of adsorption,

two kinetic models (pseudo-first-order and pseudo-second-order equation models), which are expressed by Equations (5) and (6), respectively, were applied to the experimental data.

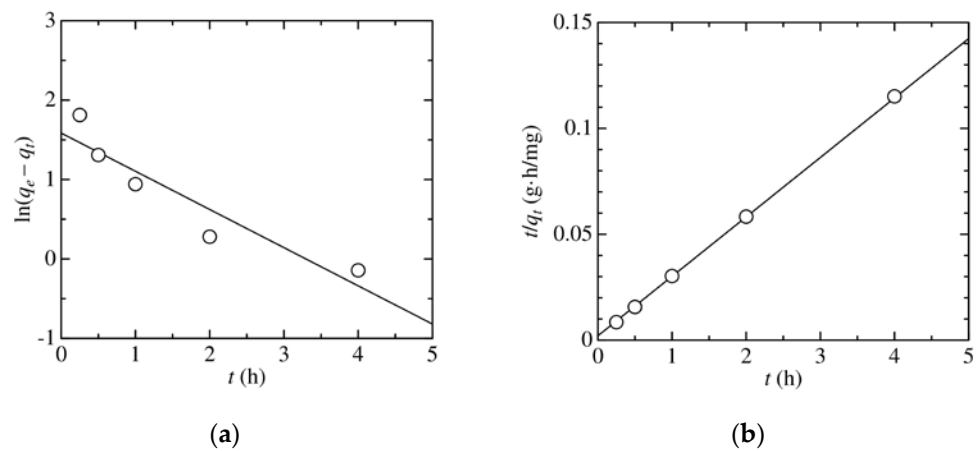
$$\ln(q_e - q_t) = \ln q_e - k_1 t \tag{5}$$

$$\frac{t}{q_t} = \frac{1}{k_2 q_e^2} + \frac{t}{q_e} \tag{6}$$

where  $k_1$  ( $\text{h}^{-1}$ ) and  $k_2$  ( $\text{g}/(\text{mg}\cdot\text{h})$ ) are the rate constants of adsorption,  $q_t$  ( $\text{mg}/\text{g}$ ) is the adsorbed amount at contact time  $t$  (h), and  $q_e$  ( $\text{mg}/\text{g}$ ) is the equilibrium uptake. As shown in Figure 12 and Table 4, the experimental data clearly fit well with the pseudo-second-order model, which indicates that the pseudo-second-order model more accurately expressed the MO adsorption kinetics than the pseudo-first-order model. The results are similar to the results reported in the literature [18,23]. This suggests that the adsorption of MO by the DA-intercalated clay is a chemisorption process, which is the rate-determining step [34,35]. The rate constant  $k_2$  of the pseudo-second-order model is relatively large compared with literature values [36–38], which resulted in a high adsorption rate and a short equilibrium arrival time, suggesting that the DA5 sample exhibits good adsorption performance.



**Figure 11.** MO adsorption of the DA5 sample as a function of contact time (dosage = 0.5 g/L, initial concentration = 20 mg/L, initial pH = 6.9, temperature = 301 K).

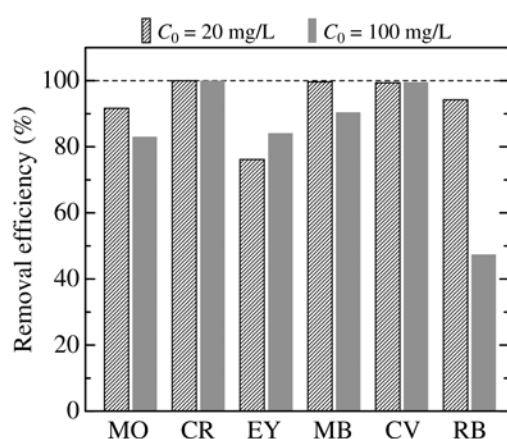


**Figure 12.** MO adsorption kinetics of the DA5 sample (dosage = 0.5 g/L, initial concentration = 20 mg/L, initial pH = 6.9, temperature = 301 K): (a) pseudo-first-order plots ( $q_e = 36 \text{ mg/g}$ ) and (b) pseudo-second-order plots.

**Table 4.** Values of parameters for MO adsorption kinetic models.

Kinetic Model	Parameter	Value
Pseudo-first-order	$q_e$ (mg/g)	4.88
	$k_1$ ( $\text{h}^{-1}$ )	0.481
	$R^2$	0.876
Pseudo-second-order	$q_e$ (mg/g)	35.2
	$k_2$ ( $\text{g}/(\text{h}\cdot\text{mg})$ )	0.524
	$R^2$	0.999

The adsorption of various dyes onto the DA5 sample was examined. The removal efficiency of the DA5 sample for the anionic and cationic dyes listed in Table 1 at initial concentrations  $C_0$  of 20 and 100 mg/L is shown in Figure 13. The DA5 sample exhibited good removability for the anionic and cationic dyes. In particular, the CR and CV dyes were almost completely removed successfully. The difference in the removal efficiency among the dyes may be attributed to variations in the hydrophobic interaction between dye and decylamine. The details are not clear at present and will be studied in future work. The FT-IR spectra of the DA5 samples after the adsorption at the initial concentration of 100 mg/L were shown in Figure 14. The DA0 and DA5 samples had typical absorption bands attributed to the hydroxyl group and alkyl chain, respectively [39,40]. The dye-loaded DA5 samples had characteristic absorption bands of each dye (indicated by the arrows in Figure 14) [41–46], which confirmed the dye adsorption. The TG/DTA curves were also illustrated in Figure 15. The DA0 sample had an endothermic peak below 100 °C which can be caused by the elimination of the adsorbed water. The DA5 sample before the adsorption had not only the endothermic peak but also an additional endothermic peak at approximately 150 °C and two exothermic peaks above 170 °C which may be attributed to the elimination and thermal decomposition of decylamine. In the dye-loaded samples, the small exothermic peak observed at 180 °C for the DA5 sample before the adsorption tended to shift toward higher temperatures while the large exothermic peak was observed around 340 °C for all the DA5 samples before and after the adsorption. Furthermore, the dye-loaded samples had an additional exothermic peak at high temperatures. As a result, the weight could decrease in a wide temperature range.

**Figure 13.** Removal efficiency of the DA5 sample for various anionic (MO, CR and EY) and cationic (MB, CV and RB) dyes at different initial concentrations (dosage = 0.5 g/L, temperature = 301 K).

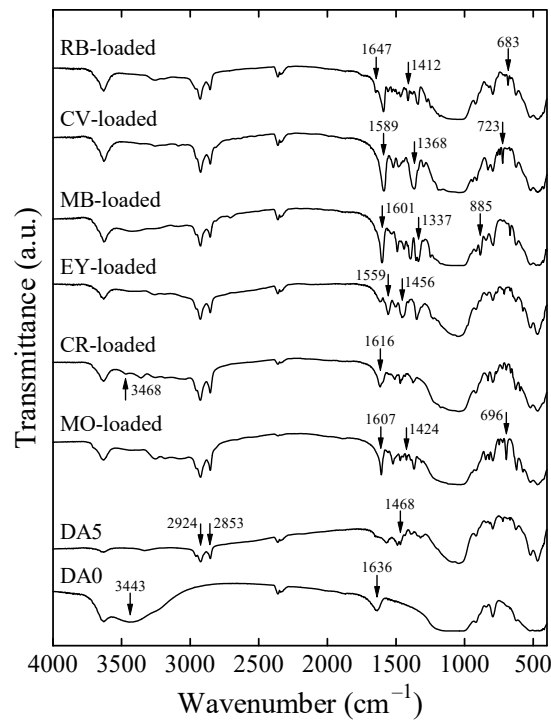


**Figure 14.** FT-IR spectra of DA0 (original acid clay) and DA5 samples after adsorption of MO, CR, EY, MB, CV and RB (dosage = 0.5 g/L, initial concentration = 100 mg/L, temperature = 301 K).

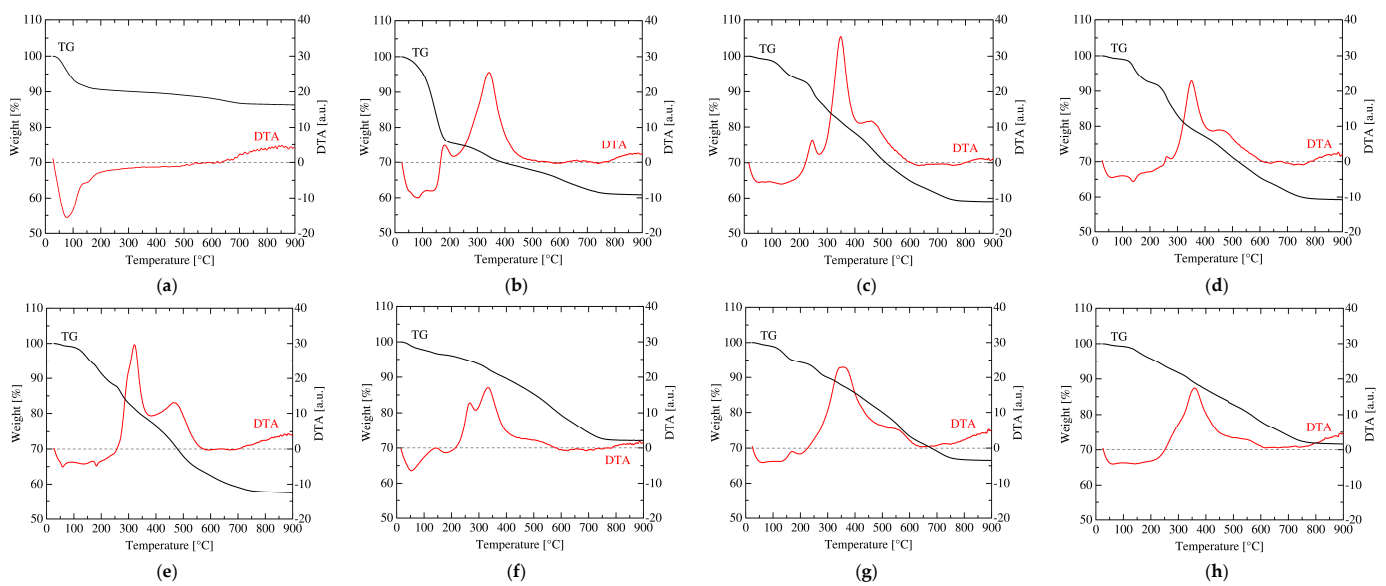


**Figure 15.** TG-DTA curves of (a) DA0 and DA5 samples (b) before adsorption and after adsorption of (c) MO, (d) CR, (e) EY, (f) MB, (g) CV and (h) RB (dosage = 0.5 g/L, initial concentration = 100 mg/L, temperature = 301 K).

Subsequently, the adsorption isotherms for MO, CR, MB, and CV, for which relatively good adsorption was observed, were further investigated. According to the variation in the equilibrium uptake  $q_e$  with the dye concentration  $C_e$  at equilibrium at various initial dye concentrations, the adsorption isotherm was analyzed by using the Langmuir model [47] and the Freundlich model [48], which are described by Equations (7) and (8), respectively.

$$\frac{C_e}{q_e} = \frac{1}{q_L K_L} + \frac{C_e}{q_m} \tag{7}$$

$$\ln q_e = \ln K_F + \frac{1}{n} \ln C_e \tag{8}$$

where  $q_L$  (mg/g) is the maximum adsorption capacity of the adsorbent,  $K_L$  (L/mg) is the Langmuir constant, and  $K_F$  (L/mg) and  $n$  (-) are the Freundlich constants. As shown in Figure 16 and Table 5, the Langmuir equation fit the experimental adsorption data well, thereby representing monolayer adsorption on a homogeneous surface.

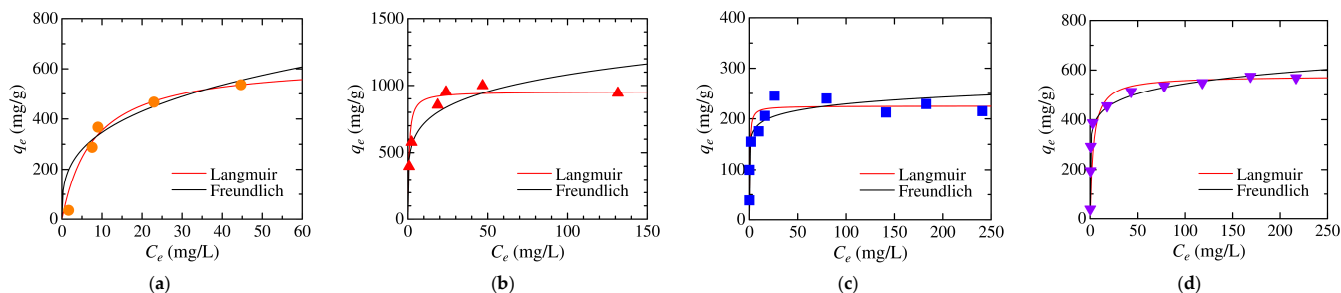


**Figure 16.** Adsorption isotherms of anionic and cationic dyes onto the DA5 sample using the Langmuir model and Freundlich model: (a) MO, (b) CR, (c) MB, and (d) CV (dosage = 0.5 g/L, temperature = 301 K).

**Table 5.** Adsorption isotherm constants of the DA5 sample for the adsorption of anionic (MO and CR) and cationic (MB and CV) dyes.

Dye	Langmuir Model			Freundlich Model		
	$q_L$ (mg/g)	$K_L$ (L/mg)	$R^2$	$K_F$ (mg/(g·(mg/L) <sup>1/n</sup> ))	$n$	$R^2$
MO	629	0.129	0.996	169	3.19	0.910
CR	954	1.386	0.999	473	5.58	0.889
MB	225	2.282	0.996	157	12.16	0.652
CV	577	0.292	0.999	327	9.02	0.974

To investigate in detail the Langmuir isotherm, a dimensionless parameter (the separation factor  $R_L$ ), which was proposed by Hall et al. [49] and is defined by Equation (9), can be used [50,51].

$$R_L = \frac{1}{1 + K_L C_0} \tag{9}$$

where  $C_0$  is the initial dye concentration. As shown in Figure 17, the  $R_L$  values for the MO, CR, MB and CV adsorption onto the DA5 sample were between 0.001 and 0.3, which were in the range of  $0 < R_L < 1$ ; hence, the DA5 sample shows satisfactory adsorption of the dyes under the specified conditions [52]. In particular,  $R_L$  for the CR, MB, and CV adsorption was below 0.01 in many experiments, suggesting that the DA5 sample undergoes an irreversible dye adsorption process over a wide range of initial dye concentrations.

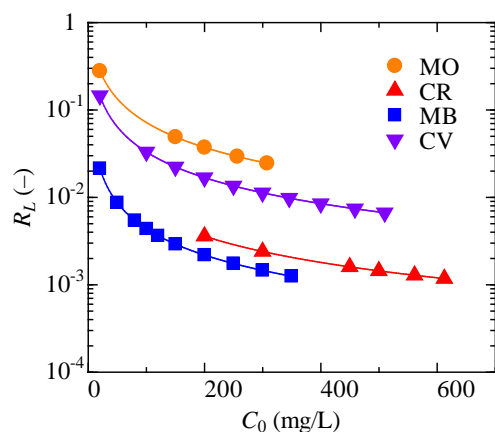


**Figure 17.** Change in the separation factor of the DA5 sample with initial concentration of anionic (MO and CR) and cationic (MB and CV) dyes (dosage = 0.5 g/L, temperature = 301 K).

The Langmuir adsorption capacities of the DA5 sample for the MO, CR, MB, and CV dyes were compared with those of various conventional adsorbents. The comparison with some recently reported literature values is shown in Table 6. Although the adsorption conditions differed from each other and some adsorbents had a maximum adsorption capacity higher than 1000 mg/g for these dyes, the DA5 sample had a high level of adsorption capacity among recently developed adsorbents including functional mesoporous silica materials with highly efficient removal of dyes [53–55]. This suggests that the DA5 sample can be widely used for the adsorption of anionic and cationic dyes.

**Table 6.** Comparison of Langmuir adsorption capacities of the DA5 sample with literature values.

Dye	Main Components of Adsorbent	$q_L$ (mg/g)	Ref.
MO	Japanese acid clay/decylamine	629	This work
	Carbon/ethylenediamine/trimethylamine	1487	[56]
	Cotton/trimethyl ammonium	645	[57]
	Carbon/Fe <sub>3</sub> O <sub>4</sub> /β-cyclodextrin/chitosan	269	[58]
	Cellulose/silica	187	[59]
	Activated carbon/chitosan	105	[60]
CR	Japanese acid clay/decylamine	954	This work
	γ-AlOOH	3881	[61]
	MgNiCo LDH	1195	[62]
	ZIF-8/MWCNT	1186	[63]
	Fe(OH) <sub>3</sub> /NiCo LDH	658	[64]
Nickel silicate	415	[65]	
MB	Japanese acid clay/decylamine	225	This work
	Limonene-derived polymer	909	[66]
	Peanut shell	538	[67]
	Bluecoke	341	[68]
	Nickel silicate	196	[65]
Holocellulose	142	[69]	
CV	Japanese acid clay/decylamine	577	This work
	Cellulose/succinic acid/choline chloride	2608	[70]
	Trithiocyanuric acid polymer	1181	[71]
	Carbon/dopamine/Fe <sub>3</sub> O <sub>4</sub> /citric acid/β-cyclodextrin	585	[72]
	MWCNT/iron oxide	165	[73]
Montmorillonite/NiFe <sub>2</sub> O <sub>4</sub> /ethylenediamine/chitosan	125	[74]	

#### 4. Conclusions

An organoclay, which consisted of Japanese acid clay and decylamine as the synthetic dye adsorbent, was successfully synthesized in a simple and cost-effective process with

low environmental impact. The structure of the organoclay changed with the decylamine content. The anionic dye (MO) removal from the aqueous solution varied depending on the structure of the organoclay; the decylamine-intercalated acid clay showed a high adsorption capacity. The adsorption conditions (dosage of adsorbent, solution pH, and temperature) for obtaining relatively high removal efficiencies were determined. Thermodynamic analysis revealed the feasibility and spontaneity of the adsorption process. The adsorption kinetics and isotherm were expressed by the pseudo-second-order equation and Langmuir models, respectively. Relatively large values of the adsorption rate constant and maximum adsorption capacity of the models suggest that the organoclay adsorbent with the decylamine-intercalated structure has good adsorption performance. The adsorbent was also found to be effective for the adsorption of various anionic and cationic dyes; in particular, Congo red and crystal violet were more effectively removed. The results suggest that the organoclay adsorbent is promising for the adsorption removal of toxic organic pollutants from wastewater.

**Funding:** This research received no external funding.

**Data Availability Statement:** Not applicable.

**Acknowledgments:** The author would like to thank T. Onizuka from Osaka Prefecture University for help with the SEM observation and M. Fukuda from Osaka Metropolitan University for help with the pore analysis.

**Conflicts of Interest:** The author declares no conflict of interest.

## References

1. Obaideen, K.; Shehata, N.; Sayed, E.T.; Abdelkareem, M.A.; Mahmoud, M.S.; Olabi, A.G. The role of wastewater treatment in achieving sustainable development goals (SDGs) and sustainability guideline. *Energy Nexus* **2022**, *7*, 100112. [[CrossRef](#)]
2. Adeola, A.O.; Abiodun, B.A.; Adenuga, D.O.; Nomngongo, P.N. Adsorptive and photocatalytic remediation of hazardous organic chemical pollutants in aqueous medium: A review. *J. Contam. Hydrol.* **2022**, *248*, 104019. [[CrossRef](#)] [[PubMed](#)]
3. Rai, P.K. Novel adsorbents in remediation of hazardous environmental pollutants: Progress, selectivity, and sustainability prospects. *Clean. Mater.* **2022**, *3*, 100054. [[CrossRef](#)]
4. Saravanan, A.; Kumar, P.S.; Hemavathy, R.V.; Jeevanantham, S.; Jawahar, M.J.; Neshanthini, J.P.; Saravanan, R. A review on synthesis methods and recent applications of nanomaterial in wastewater treatment: Challenges and future perspectives. *Chemosphere* **2022**, *307*, 135713. [[CrossRef](#)]
5. Teo, S.H.; Ng, C.H.; Islam, A.; Abdulkareem-Alsultan, G.; Joseph, C.G.; Janaun, J.; Taufiq-Yap, Y.H.; Khandaker, S.; Islam, G.J.; Znad, H.; et al. Sustainable toxic dyes removal with advanced materials for clean water production: A comprehensive review. *J. Clean. Prod.* **2022**, *332*, 130039. [[CrossRef](#)]
6. Lan, D.; Zhu, H.; Zhang, J.; Li, S.; Chen, Q.; Wang, C.; Wu, T.; Xu, M. Adsorptive removal of organic dyes via porous materials for wastewater treatment in recent decades: A review on species, mechanisms and perspectives. *Chemosphere* **2022**, *293*, 133464. [[CrossRef](#)]
7. Sultana, M.; Rownok, M.H.; Sabrin, M.; Rahaman, M.H.; Nur Alam, S.M. A review on experimental chemically modified activated carbon to enhance dye and heavy metals adsorption. *Cleaner Eng. Technol.* **2022**, *6*, 100382. [[CrossRef](#)]
8. Sutar, S.; Patil, P.; Jadhav, J. Recent advances in biochar technology for textile dyes wastewater remediation: A review. *Environ. Res.* **2022**, *209*, 112841. [[CrossRef](#)]
9. Adel, M.; Ahmed, M.A.; Elabiad, M.A.; Mohamed, A.A. Removal of heavy metals and dyes from wastewater using graphene oxide-based nanomaterials: A critical review. *Environ. Nanotechnol. Monit. Manag.* **2022**, *18*, 100719. [[CrossRef](#)]
10. De Magalhães, L.F.; Da Silva, G.R.; Peres, A.E.C. Zeolite application in wastewater treatment. *Adsorp. Sci. Technol.* **2022**, *2022*, 4544104. [[CrossRef](#)]
11. Abdel Rahman, R.O.; El-Kamash, A.M.; Hung, Y.-T. Applications of nano-zeolite in wastewater treatment: An overview. *Water* **2022**, *14*, 137. [[CrossRef](#)]
12. Sriram, G.; Bendre, A.; Mariappan, E.; Altalhi, T.; Kigga, M.; Ching, Y.C.; Jung, H.-Y.; Bhaduri, B.; Kurkuri, M. Recent trends in the application of metal-organic frameworks (MOFs) for the removal of toxic dyes and their removal mechanism—A review. *Sustain. Mater. Technol.* **2022**, *31*, e00378. [[CrossRef](#)]
13. Jaria, G.; Calisto, V.; Esteves, V.I.; Otero, M. Overview of relevant economic and environmental aspects of waste-based activated carbons aimed at adsorptive water treatments. *J. Clean. Prod.* **2022**, *344*, 130984. [[CrossRef](#)]
14. Zhang, T.; Wang, W.; Zhao, Y.; Bai, H.; Wen, T.; Kang, S.; Song, G.; Song, S.; Komarneni, S. Removal of heavy metals and dyes by clay-based adsorbents: From natural clays to 1D and 2D nano-composites. *Chem. Eng. J.* **2021**, *420*, 127574. [[CrossRef](#)]

15. Kausor, M.A.; Gupta, S.S.; Bhattacharyya, K.G.; Chakraborty, D. Montmorillonite and modified montmorillonite as adsorbents for removal of water soluble organic dyes: A review on current status of the art. *Inorg. Chem. Commun.* **2022**, *143*, 109686. [[CrossRef](#)]
16. Liu, B.; Wang, X.; Yang, B.; Sun, R. Rapid modification of montmorillonite with novel cationic Gemini surfactants and its adsorption for methyl orange. *Mater. Chem. Phys.* **2011**, *130*, 1220–1226. [[CrossRef](#)]
17. Kan, T.; Jiang, X.; Zhou, L.; Yang, M.; Duan, M.; Liu, P.; Jiang, X. Removal of methyl orange from aqueous solutions using a bentonite modified with a new gemini surfactant. *Appl. Clay Sci.* **2011**, *54*, 184–187. [[CrossRef](#)]
18. Luo, Z.; Gao, M.; Ye, Y.; Yang, S. Modification of reduced-charge montmorillonites by a series of Gemini surfactants: Characterization and application in methyl orange removal. *Appl. Surf. Sci.* **2015**, *324*, 807–816. [[CrossRef](#)]
19. Liang, Y.; Li, H. A comparison of trimeric surfactant intercalated montmorillonite with its gemini modified one: Characterization and application in methyl orange removal. *J. Mol. Liq.* **2017**, *227*, 139–146. [[CrossRef](#)]
20. Belhouchat, N.; Zaghouane-Boudiaf, H.; Viseras, C. Removal of anionic and cationic dyes from aqueous solution with activated organo-bentonite/sodium alginate encapsulated beads. *Appl. Clay Sci.* **2017**, *135*, 9–15. [[CrossRef](#)]
21. Ren, H.-P.; Tian, S.-P.; Zhu, M.; Zhao, Y.-Z.; Li, K.-X.; Ma, Q.; Ding, S.-Y.; Gao, J.; Miao, Z. Modification of montmorillonite by Gemini surfactants with different chain lengths and its adsorption behavior for methyl orange. *Appl. Clay Sci.* **2018**, *151*, 29–36. [[CrossRef](#)]
22. Gamoudi, S.; Srasra, E. Removal of cationic and anionic dyes using purified and surfactant-modified Tunisian clays: Kinetic, isotherm, thermodynamic and adsorption–mechanism studies. *Clay Miner.* **2018**, *53*, 159–174. [[CrossRef](#)]
23. Peng, S.; Mao, T.; Zheng, C.; Wu, X.; Wei, Y.; Zeng, Z.; Xiao, R.; Sun, Y. Polyhydroxyl gemini surfactant-modified montmorillonite for efficient removal of methyl orange. *Colloids Surf. A Physicochem. Eng. Asp.* **2019**, *578*, 123602. [[CrossRef](#)]
24. Saavedra-Labastida, E.; Díaz-Nava, M.C.; Illescas, J.; Muro, C. Comparison of the removal of an anionic dye from aqueous solutions by adsorption with organically modified clays and their composites. *Water Air Soil Pollut.* **2019**, *230*, 88. [[CrossRef](#)]
25. Iwasaki, T. Structure of a layered octosilicate intercalated with alkylamines with different molecular structures in water. *J. Solid State Chem.* **2020**, *290*, 121545. [[CrossRef](#)]
26. Sasaki, S. Studies on Japanese acid earth. *Soil Sci. Plant Nutr.* **1955**, *1*, 7–8. [[CrossRef](#)]
27. Sasaki, R.; Takahashi, N.; Sakao, K.; Goto, T. Adsorption of zearalenone to Japanese acid clay and influencing factors. *Mycotoxin Res.* **2014**, *30*, 33–41. [[CrossRef](#)]
28. Hayakawa, T.; Oya, M.; Minase, M.; Fujita, K.; Teepakakorn, A.; Ogawa, M. Preparation of sodium-type bentonite with useful swelling property by a mechanochemical reaction from a weathered bentonite. *Appl. Clay Sci.* **2019**, *175*, 124–129. [[CrossRef](#)]
29. Iwasaki, T. Effect of solvents on the direct intercalation of decylamine into H-octosilicate. *Appl. Clay Sci.* **2020**, *199*, 105882. [[CrossRef](#)]
30. Kwon, O.-Y.; Park, K.-W. Intercalation behavior of dodecylamine into layered silicates in organic solvents. *J. Ind. Eng. Chem.* **2001**, *7*, 44–49.
31. Lagaly, G. Interaction of alkylamines with different types of layered compounds. *Solid State Ion.* **1986**, *22*, 43–51. [[CrossRef](#)]
32. Fu, S.; Sun, Z.; Huang, P.; Li, Y.; Hu, N. Some basic aspects of polymer nanocomposites: A critical review. *Nano Mater. Sci.* **2019**, *1*, 2–30. [[CrossRef](#)]
33. Boukhemkhem, A.; Pizarro, A.H.; Molina, C.B. Enhancement of the adsorption properties of two natural bentonites by ion exchange: Equilibrium, kinetics and thermodynamic study. *Clay Miner.* **2020**, *55*, 132–141. [[CrossRef](#)]
34. Agcaoili, A.R.; Herrera, M.U.; Futalan, C.M.; Balela, M.D.L. Fabrication of polyacrylonitrile-coated kapok hollow microtubes for adsorption of methyl orange and Cu(II) ions in aqueous solution. *J. Taiwan Inst. Chem. Eng.* **2017**, *78*, 359–369. [[CrossRef](#)]
35. Gamoudi, S.; Srasra, E. Adsorption of organic dyes by HDPy<sup>+</sup>-modified clay: Effect of molecular structure on the adsorption. *J. Mol. Struct.* **2019**, *1193*, 522–531. [[CrossRef](#)]
36. Hua, T.; Li, D.; Li, X.; Lin, J.; Niu, J.; Cheng, J.; Zhou, X.; Hu, Y. Synthesis of mesoporous-structured MIL-68(Al)/MCM-41-NH<sub>2</sub> for methyl orange adsorption: Optimization and selectivity. *Environ. Res.* **2022**, *215*, 114433. [[CrossRef](#)]
37. Zhu, B.; Xu, J.; Xu, Z.; Wu, M.; Jiang, H. Soft-template solvent thermal method synthesis of magnetic mesoporous carbon–silica composite for adsorption of methyl orange from aqueous solution. *Environ. Sci. Pollut. Res.* **2022**, *29*, 40734–40744. [[CrossRef](#)]
38. Hajipour, N.; Ghorbanpour, M.; Safajou-jahankhanemlou, M. Synthesis and characterization of solid-state Fe-exchanged nanobentonite and evaluation of methyl orange adsorption. *Environ. Sci. Pollut. Res.* **2022**, *29*, 49898–49907. [[CrossRef](#)]
39. Horri, N.; Sanz-Pérez, E.S.; Arencibia, A.; Sanz, R.; Frini-Srasra, N.; Srasra, E. Effect of acid activation on the CO<sub>2</sub> adsorption capacity of montmorillonite. *Adsorption* **2020**, *26*, 793–811. [[CrossRef](#)]
40. Okamoto, H.; Kumai, Y.; Sugiyama, Y.; Mitsuoka, T.; Nakanishi, K.; Ohta, T.; Nozaki, H.; Yamaguchi, S.; Shirai, S.; Nakano, H. Silicon nanosheets and their self-assembled regular stacking structure. *J. Am. Chem. Soc.* **2010**, *132*, 2710–2718. [[CrossRef](#)]
41. Shen, T.; Jiang, C.; Wang, C.; Sun, J.; Wang, X.; Li, X. A TiO<sub>2</sub> modified abiotic–biotic process for the degradation of the azo dye methyl orange. *RSC Adv.* **2015**, *5*, 58704–58712. [[CrossRef](#)]
42. Chen, Y.; Chen, S.; Deng, Z.; Xu, X.; Qin, J.; Guo, X.; Bai, Z.; Chen, X.; Lu, Z. Fabrication of polystyrene/CuO@calcined layered double hydroxide microspheres with high adsorption capacity for Congo red. *Colloids Surf. A Physicochem. Eng. Asp.* **2022**, *652*, 129827. [[CrossRef](#)]

43. Azmi, S.N.H.; Al-Fazari, A.; Al-Badaei, M.; Al-Mahrazi, R. Utility of eosin Y as a complexing reagent for the determination of citalopram hydrobromide in commercial dosage forms by fluorescence spectrophotometry. *Luminescence* **2015**, *30*, 1352–1359. [[CrossRef](#)] [[PubMed](#)]
44. Alshehri, A.A.; Malik, M.A. Biogenic fabrication of ZnO nanoparticles using *Trigonella foenum-graecum* (Fenugreek) for proficient photocatalytic degradation of methylene blue under UV irradiation. *J. Mater. Sci. Mater. Electron.* **2019**, *30*, 16156–16173. [[CrossRef](#)]
45. Sulthana, R.; Taqui, S.N.; Syed, U.T.; Soudagar, M.E.M.; Mujtaba, M.A.; Mir, R.A.; Shahapurkar, K.; Khidmatgar, A.; Mohanavel, V.; Syed, A.A.; et al. Biosorption of crystal violet by nutraceutical industrial fennel seed spent equilibrium, kinetics, and thermodynamic studies. *Biocatal. Agric. Biotechnol.* **2022**, *43*, 102402. [[CrossRef](#)]
46. Jiang, Z.; Dong, B.; Chen, B.; Wang, J.; Xu, L.; Zhang, S.; Song, H. Multifunctional Au@mSiO<sub>2</sub>/rhodamine B isothiocyanate nanocomposites: Cell imaging, photocontrolled drug release, and photothermal therapy for cancer cells. *Small* **2013**, *9*, 604–612. [[CrossRef](#)] [[PubMed](#)]
47. Langmuir, I. The adsorption of gases on plane surfaces of glass, mica and platinum. *J. Am. Chem. Soc.* **1918**, *40*, 1361–1403. [[CrossRef](#)]
48. Freundlich, H. Über die Adsorption in Lösungen. *Z. Phys. Chem.* **1907**, *57*, 385–470. [[CrossRef](#)]
49. Hall, K.R.; Eagleton, L.C.; Acrivos, A.; Vermeulen, T. Pore- and solid-diffusion kinetics in fixed-bed adsorption under constant-pattern conditions. *Ind. Eng. Chem. Fundam.* **1966**, *5*, 212–223. [[CrossRef](#)]
50. Vimonses, V.; Lei, S.; Jin, B.; Chow, C.W.K.; Saint, C. Kinetic study and equilibrium isotherm analysis of Congo red adsorption by clay materials. *Chem. Eng. J.* **2009**, *148*, 354–364. [[CrossRef](#)]
51. Hameed, B.H. Spent tea leaves: A new non-conventional and low-cost adsorbent for removal of basic dye from aqueous solutions. *J. Hazard. Mater.* **2009**, *161*, 753–759. [[CrossRef](#)] [[PubMed](#)]
52. El-Gamal, S.M.A.; Amin, M.S.; Ahmed, M.A. Removal of methyl orange and bromophenol blue dyes from aqueous solution using Sorel's cement nanoparticles. *J. Environ. Chem. Eng.* **2015**, *3*, 1702–1712. [[CrossRef](#)]
53. Chueachot, R.; Wongkhueng, S.; Khankam, K.; Lakrathok, A.; Kaewnon, T.; Naowanon, W.t.; Amnuaypanich, S.; Nakhong, R. Adsorption efficiency of methylene blue from aqueous solution with amine-functionalized mesoporous silica nanospheres by co-condensation biphasic synthesis: Adsorption condition and equilibrium studies. *Mater. Today Proc.* **2018**, *5*, 14079–14085. [[CrossRef](#)]
54. Nicola, R.; Muntean, S.-G.; Nistor, M.-A.; Putz, A.-M.; Almásy, L.; Săcărescu, L. Highly efficient and fast removal of colored pollutants from single and binary systems, using magnetic mesoporous silica. *Chemosphere* **2022**, *261*, 127737. [[CrossRef](#)]
55. Nicola, R.; Costișor, O.; Muntean, S.-G.; Nistor, M.-A.; Putz, A.-M.; Ianăși, C.; Lazău, R.; Almásy, L.; Săcărescu, L. Mesoporous magnetic nanocomposites: A promising adsorbent for the removal of dyes from aqueous solutions. *J. Porous Mater.* **2020**, *27*, 413–428. [[CrossRef](#)]
56. Liu, M.; Zheng, J.; Wang, L.; Hu, Z.; Lan, S.; Rao, W.; Liu, Y.; Xie, Y.; Yu, C. Ultrafast and selective adsorption of anionic dyes with amine-functionalized glucose-based adsorbents. *J. Mol. Struct.* **2022**, *1263*, 133150. [[CrossRef](#)]
57. Du, J.; Zhang, M.; Dong, Z.; Yang, X.; Xiong, H.; Zeng, Z.; Chen, Z.; Zhao, L. Facile fabrication of quaternary ammonium salt modified cotton linter by radiation grafting and its effective removal of methyl orange: Batch and dynamic flow mode studies. *Fibers Polym.* **2022**, *23*, 925–934. [[CrossRef](#)]
58. Li, K.; Li, X.; Li, B. Investigation the adsorption behavior of functional carbon-based composites for efficient removing anions/cations in single and multicomponent systems. *Sep. Purif. Technol.* **2022**, *289*, 120737. [[CrossRef](#)]
59. Grishkewich, N.; Li, Y.; Liu, K.; Tam, K.C. Synthesis and characterization of modified cellulose nanofibril organosilica aerogels for the removal of anionic dye. *J. Polym. Res.* **2022**, *29*, 261. [[CrossRef](#)]
60. Kamdod, A.S.; Kumar, M.V.P. Adsorption of methylene blue, methyl orange, and crystal violet on microporous coconut shell activated carbon and its composite with chitosan: Isotherms and kinetics. *J. Polym. Environ.* **2022**, *in press*. [[CrossRef](#)]
61. Wang, D.; Li, Z.; Lv, F.; Chen, J.; Wu, C.; Li, Y.; Li, Y.; Shen, J. Synthesis of nucleoshell  $\gamma$ -AlOOH as an ultra-high-capacity adsorbent for organic pollutants removal. *Colloid Interface Sci. Commun.* **2022**, *50*, 100658. [[CrossRef](#)]
62. Wang, X.; Cheng, B.; Zhang, L.; Yu, J.; Li, Y. Synthesis of MgNiCo LDH hollow structure derived from ZIF-67 as superb adsorbent for Congo red. *J. Colloid Interface Sci.* **2022**, *612*, 598–607. [[CrossRef](#)] [[PubMed](#)]
63. Zhang, X.; Yuan, N.; Xu, S.; Li, Y.; Wang, Q. Efficient adsorptive elimination of organic pollutants from aqueous solutions on ZIF-8/MWCNTs-COOH nanoadsorbents: Adsorption kinetics, isotherms, and thermodynamic study. *J. Ind. Eng. Chem.* **2022**, *111*, 155–167. [[CrossRef](#)]
64. Liu, L.; Xia, Z.-Q.; Li, S.-B.; Zhang, Y.-J.; Wang, N. MOF-derived double-shelled Fe(OH)<sub>3</sub>@NiCo-LDH hollow cubes and their efficient adsorption for anionic organic pollutant. *J. Porous Mater.* **2022**, *29*, 931–945. [[CrossRef](#)]
65. Jia, Z.; Han, C.; Wu, L.; Zhang, D.; Li, M. Biotemplated synthesis of hollow nickel silicate fiber for organic dye contaminants and its selective adsorption. *Colloids Surf. A Physicochem. Eng. Asp.* **2022**, *648*, 129219. [[CrossRef](#)]
66. Wei, X.; Deng, S.; Chen, D.; Wang, L.; Yang, W. Limonene-derived hollow polymer particles: Preparation and application for the removal of dyes and heavy metal ions. *J. Polym. Sci.* **2022**, *60*, 2572–2581. [[CrossRef](#)]
67. Du, P.; Xu, L.; Ke, Z.; Liu, J.; Wang, T.; Chen, S.; Mei, M.; Li, J.; Zhu, S. A highly efficient biomass-based adsorbent fabricated by graft copolymerization: Kinetics, isotherms, mechanism and coadsorption investigations for cationic dye and heavy metal. *J. Colloid Interface Sci.* **2022**, *616*, 12–22. [[CrossRef](#)]

68. Yang, R.; Zhou, J.; Wu, L.; Zhang, Q.; Song, Y. Understanding effects of potassium activator on the porous structure and adsorption performance of bluecoke-based porous powder during microwave heating. *J. Mol. Liq.* **2022**, *366*, 120249. [[CrossRef](#)]
69. Radjai, M.; Ferkous, H.; Jebali, Z.; Majdoub, H.; Bourzami, R.; Raffin, G.; Achour, M.; Gil, A.; Boutahala, M. Adsorptive removal of cationic and anionic dyes on a novel mesoporous adsorbent prepared from diatomite and anionic cellulose nanofibrils: Experimental and theoretical investigations. *J. Mol. Liq.* **2022**, *361*, 119670. [[CrossRef](#)]
70. Martins, L.R.; Soares, L.C.; Gurgel, L.V.A.; Gil, L.F. Use of a new zwitterionic cellulose derivative for removal of crystal violet and orange II from aqueous solutions. *J. Hazard. Mater.* **2022**, *424*, 127401. [[CrossRef](#)]
71. Kim, S.; Tang, K.; Kim, T.-H.; Hwang, Y. Selective removal of cationic organic pollutants using disulfide-linked polymer. *Sep. Purif. Technol.* **2022**, *288*, 120522. [[CrossRef](#)]
72. Yan, J.; Li, K.; Yan, J.; Fang, Y.; Liu, B. A magnetically recyclable magnetic graphite oxide composite functionalized with polydopamine and  $\beta$ -cyclodextrin for cationic dyes wastewater remediation: Investigation on adsorption performance, reusability and adsorption mechanism. *Appl. Surf. Sci.* **2022**, *602*, 154338. [[CrossRef](#)]
73. Song, G.; Shi, Y.; Wang, H.; Li, A.; Li, W.; Sun, Y.; Ding, G. Effective sorptive removal of five cationic dyes from aqueous solutions by using magnetic multi-walled carbon nanotubes. *Water Sci. Technol.* **2022**, *85*, 1999–2014. [[CrossRef](#)]
74. Gomaa, H.; Abd El-Monaem, E.M.; Eltaweil, A.S.; Omer, A.M. Efficient removal of noxious methylene blue and crystal violet dyes at neutral conditions by reusable montmorillonite/ $\text{NiFe}_2\text{O}_4$ @amine-functionalized chitosan composite. *Sci. Rep.* **2022**, *12*, 15499. [[CrossRef](#)]

**Disclaimer/Publisher's Note:** The statements, opinions and data contained in all publications are solely those of the individual author(s) and contributor(s) and not of MDPI and/or the editor(s). MDPI and/or the editor(s) disclaim responsibility for any injury to people or property resulting from any ideas, methods, instructions or products referred to in the content.